Journal of Alloys and Compounds 655 (2016) 357–363

Contents lists available at ScienceDirect

Journal of Alloys and Compounds

journal homepage: http://www.elsevier.com/locate/jalcom

Onset of plasticity and its relation to atomic structure in CuZr metallic glass nanowire: A molecular dynamics study

Matías Sepúlveda-Macías*, Nicolás Amigo, Gonzalo Gutiérrez

Grupo de NanoMateriales, Departamento de Física, Facultad de Ciencias, Universidad de Chile, Casilla 653, Santiago, Chile

ARTICLE INFO

Article history:
Received 20 July 2015
Accepted 15 September 2015
Available online 25 September 2015

Keywords:
Amorphous materials
Metallic glasses
Mechanical properties
Computer simulations
Molecular dynamics simulations

ABSTRACT

We present a computational tensile test which shows the evolution of the atomic structure of a $Cu_{50}Zr_{50}$ metallic glass nanowire at 300 K as the applied strain increases. The system consists of a parallelepiped composed by 1.008.000 atoms interacting by means of an embedded atom potential. The local structure of the atoms is analyzed using the Voronoi polyhedral technique and the nucleation and propagation of the shear band by monitoring the local atomic shear strain. Our results clearly reveal three regimes: an elastic regime below 4% of strain, a homogeneous deformation, where the shear band begins to form, and an inhomogeneous deformation regime, above 10% of strain, where the shear band is formed. Each regime is characterized by a typical bimodal polyhedra distribution, except at 10% of strain, where the distribution is unimodal. A detailed atomic level study of the shear band shows that, in spite of the large displacement experimented by each atom with respect to its environment, its short range order is similar to the regions outside the shear band.

1. Introduction

Metallic Glasses (MGs) are among the most actively studied metallic materials, both from the experimental and theoretical point of view, because of their technological promise for practical applications and scientific importance in understanding glass formation and glass phenomena [1]. Thanks to the bulk size of the sample, it became possible to investigate the mechanical, physical and chemical properties of metallic glasses systematically. Several are the lines of research on MGs nowadays, including glass formation, practical applications and mechanical properties. In particular, atomic level explanation of the mechanism of elastic–-plastic regime is currently the subject of intense research. For instance, metallic glasses have much higher yield point σ_y and larger elastic strain limit ε_y (in both cases, more than an order of magnitude greater) with respect to their crystalline counterpart, which is thought to be a consequence of the difference in the deformation and fracture mechanisms between metallic glass and crystalline alloys. Moreover, it has been demonstrated that these apparent values for σ_y and ε_y, though high, are actually not the ceiling, or ideal limit, for MGs. Recently, using sub-micron sized MGs samples, Tian et al. [2,3] showed these values can be about twice as high as values observed in bulk metallic glass samples.

It is well known that bulk metallic glasses, in addition to the high yield strength and an elastic deformation to a strain limit about 2% (for instance, in the case of CuZr MG the yield strength can be as high as 2 GPa with an uniaxial elastic strain limit of 2%), show very little ductility at room temperature [2]. Amorphous metals lack the tensile ductility and this is one of the main problem that prevent practical applications [4]. Thus, an understanding of the elastic–plastic behavior is needed. In contrast, the general mechanism of plastic deformation of crystalline metals is well understood. It is known that this regime is mainly mediated by the nucleation and propagation of dislocations as well as by grain boundary sliding. This has been shown in experimental and computational studies [5–7]. In metallic glasses (MGs), on the other hand, the plastic behavior is quite different from their crystalline counterparts and a relationship between atomic-micro structure and properties remain one of the barriers that has hampered the progress to wide application of MG [8]. It has been hypothesized that the plasticity is initiated by structural and dynamical heterogeneities called shear transformation zones (STZs). They lead to the generation of free volume and the nucleation of shear bands (SBs), which are characterized by a more strained, less dense structure than the glass matrix [9–12].

* Corresponding author.
E-mail addresses: msepmacias@gmail.com (M. Sepúlveda-Macías), nicorafa@gmail.com (N. Amigo), gonzalogutierr@gmail.com (G. Gutiérrez).

http://dx.doi.org/10.1016/j.jallcom.2015.09.149
0925-8388/

However, macroscopic MGs are not ductile. The elastic energy stored in a millimeter-sized sample, subject to stress, is large enough to nucleate quickly a catastrophic SB causing the rupture of the MG [13,14]. Nevertheless, when decreasing the volume of the sample, the stored elastic energy decreases faster than the energy of the area associated with the localized shear, slowing the shear banding process and making it less violent, thus avoiding a catastrophic failure of the material. Hence, following experiments, as well as computational simulations, ductility is observed in submicron-sized MGs [3,15,16].

Many studies have been carried out during the past years in order to understand the SBs nucleation, as well as to connect them to the well known defects given in crystalline metals [17,18,2,19,20]. In particular it would be desirable to have studies which directly relate the evolution of the SBs and glass matrix structure to each step of the applied strain, which would allow us to easily connect the evolution of the atomic structure to the stress–strain curve. Here we present a molecular dynamic study which shows the evolution of the atomic structure of a $Cu_{50}Zr_{50}$ metallic glass nanowire at 300 K according to the applied strain via a tensile test. The local structure of atoms is analyzed in detail by means of the Voronoi polyhedra and the nucleation and propagation of SBs by means of the atomic strain.

The paper is organized as follows: In Section 2 we explain the simulation procedure, including the inter-atomic potential and tools employed. In Section 3 we present the results for the tensile test and the respective analysis. Finally in Section 4 we draw the conclusions.

2. Methodology

In order to study CuZr metallic glass system using molecular dynamics simulations, it is important to choose an adequate inter-atomic potential to accurately describe the physical properties. Here, we adopt the embedded-atom potential (EAM) proposed by Mendelev et al. for the CuZr system [21,22], since it mimics reasonably well the mechanical behavior of the system, and it has been widely used and accepted when studying CuZr metallic glasses [23,24,18,19]. The EAM gives the total energy of an atomic system in the form [25,26].

$$U = \sum_{i=1}^{N-1} \sum_{j=i+1}^{N} \phi_{t_i t_j}(r_{ij}) + \sum_{i=1}^{N} \Phi_{t_i}(\rho_i), \tag{1}$$

where t_i is the elemental type of atom i, $\phi_{t_i t_j}(r_{ij})$ is the pair potential between atoms i and j separated by a distance r_{ij} and Φ_{t_i} is the embedding energy function of atom i in an electron density ρ_i, given by

$$\rho_i = \sum_{j} \psi_{t_i t_j}(r_{ij}). \tag{2}$$

The $Cu_{50}Zr_{50}$ metallic glass is prepared using a procedure similar to the one proposed by Wang et al. [27]. First, a crystalline CuZr b2 system with dimensions of L_x, L_y, L_z = 90.72, 38.88, 38.88 Å, composed of 8064 atoms is created. Using periodic boundary conditions (PBC) in all three directions, the temperature and pressure are set at 2000 K and 0 GPa respectively, allowing the system to relax for 2 ns using the NPT ensemble [28]. The integration time step is set at 1 fs. Then, the system is cooled down to 300 K using the following procedure. The first step consists in reducing the temperature by 25 K over 2000 fs using the Berendsen thermostat and keeping the pressure at zero using the Berendsen barostat [29]. In the second step, the system is allowed to relax for 500,000 fs using the NPT ensemble. These two steps are repeated consecutively until a relaxed amorphous system at 300 K and zero pressure is reached after 68 iterations. Hence, the calculated cooling rate is 5×10^{10} K/s.

The obtained system is a $Cu_{50}Zr_{50}$ metallic glass composed of 8064 atoms. In order to generate a bigger metallic glass nanowire, the system is replicated five times in each direction, giving a total of 1.008.000 atoms with dimensions of L_x, L_y, L_z = 453.6, 194.4, 194.4 Å. Free boundary conditions are set in y and z directions, and PBC are kept in the x direction. This new system is allowed to relax for 100,000 fs to ensure a well-equilibrated sample. With this system at hand, we perform the tensile test by loading the axial direction of the system, as shown in Fig. 2(a), at a strain rate of 5×10^8 s^{-1}. For this purpose, the positions of atoms are rescaled each time step. The temperature is kept constant at 300 K during the whole procedure. The molecular dynamics simulation is carried out using the classical molecular dynamics code LAMMPS [30] and the visualization by means of OVITO [31]. Some analysis were performed using the tools provided by LPMD code [32].

The structural changes of the sample generated during the tensile test, are characterized by using the local atomic shear strain, η_i, implemented in OVITO, defined by Shimizu et al. [17] as

$$\eta_i = \sqrt{\eta_{yz}^2 + \eta_{xz}^2 + \eta_{xy}^2 + \frac{(\eta_{yy} - \eta_{zz})^2 + (\eta_{xx} - \eta_{zz})^2 + (\eta_{xx} - \eta_{yy})^2}{6}}, \tag{3}$$

where $\eta_{\alpha\beta}$ are the components of the strain tensor of atom i. The region where the local atomic shear strain is less than 0.3 are called unstrained regions or metallic glass matrix. The region where the local atomic shear strain is greater than 0.3 are called strained regions. These regions comprise the SB, which is identified by visual inspection.

The Voronoi polyhedra analysis is used to study the local structure of the sample, both the strained region and the unstrained, metallic glass matrix. The analysis is done with the C++ library VORO++, developed by Rycroft [33].

3. Results

3.1. Stress–strain curves

The stress–strain curve for amorphous $Cu_{50}Zr_{50}$ is shown in Fig. 1. It can be seen that there is an elastic behavior up to 4%. Between 4% and 6% there is an homogeneous deformation zone, and over 6% starts the inhomogeneous zone. Note that around 12% of strain there is an inflection point in the stress–strain curve. The tensile and flow stress are around 1.98 GPa and 1.14 GPa respectively. In Fig. 2 we display a cross-section view of the whole sample at four different strain percentages, where atoms are colored according to their local atomic shear strain. Fig. 3 shows the same situation but in this case the atoms with a local atomic shear strain lower than 0.3 were deleted. In Fig. 2(a) we present the initial condition, where all the atoms are around their initial positions and this behavior holds until about 4%. After that, some atoms begin to cross the threshold of 0.3 shear strain. Of course this situation also appear in Fig. 3(a) where the simulation cell is empty. Fig. 2(b) corresponds to a strain of 6%. Here clusters of atoms which have a local atomic shear strain greater than 0.3 (shown by light blue) appear at the surface. These clusters are STZs which are not only in the surface but also in the bulk, as is displayed in Fig. 3(b). As the strain increases these STZs propagate, coalesce, and nucleate becoming SB, as can be seen in Fig. 2(c) at the left part of the sample. After that, the SB develops, weakening the sample in that region, where it eventually fail.

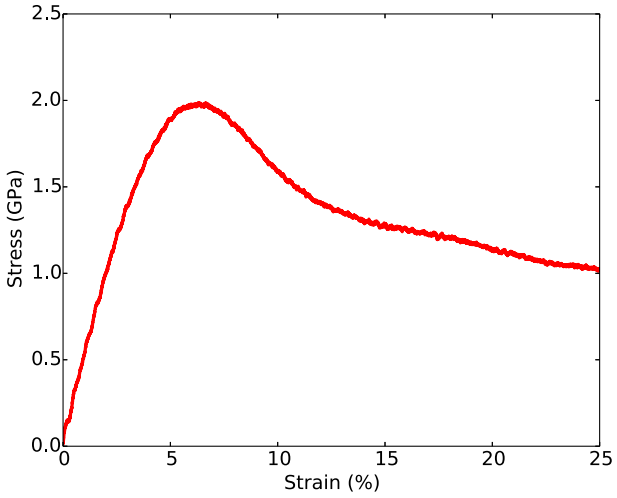

Fig. 1. Room-temperature stress–strain curve for $Cu_{50}Zr_{50}$ metallic glass under tensile deformation.

In the following we will characterize the structure at an atomic level, showing the different local structures that appear in each stage described above.

3.2. Atomic level structure according to strain evolution

The atomic level structure underlying the changes suffered by the structure allow us to have an insight about the mechanism of STZs formation and their evolution to SB [34]. This analysis is done by identifying the short range order (SRO) and the building blocks of the sample. For that purpose we use Voronoi analysis, a useful tool employed in MGs research.

The Voronoi analysis is a tessellation method that consists of dividing the 3-D space into cells centered in each atom, in the same way as one obtains the Wigner–Seitz primitive cell in solid state physics. In our case we link each atom with a Voronoi polyhedral index that is expressed as $<n_3, n_4, n_5, n_6>$, where n_i denotes the number of i-edged faces of the Voronoi polyhedron. In that way the arrangement and symmetry of the nearest-neighbor atoms around the center atom is described. This analysis is carried out using Voro++ software [33].

We analyze two aspects of the evolution of polyhedra with respect to strain. Firstly, we monitor the change of the total number of different classes of polyhedra, ordered according to the number of faces. That is, for example at 0% of strain there are 34 different classes of polyhedra: the class of 12 faces, the class of 13 faces, up to the class of 47 faces. Secondly, for each class there are different types of polyhedra according to the kind of faces that compose them. For example, in the class of 12 faces polyhedra, there is a polyhedron composed only by pentagonal faces, with Voronoi index ⟨0, 0, 12, 0⟩; other composed by square, pentagonal and hexagonal faces, with index ⟨0, 2, 8, 2⟩; and other kind of polyhedra with its respective Voronoi indices.

The first observation is that as strain is applied, the number of different classes of polyhedra decreases, from 34 classes at 0% strain to 27 classes at 25% strain, as it can be seen in Table 1. We can observe that near the 6% of strain, which is the maximum in the stress–strain curve, occurs a transition from 12-face class to 13-face class. Beyond 13% of strain, where the SB is already formed, the predominant class is the 13-face polyhedra, in particular the triskaidecahedra characterized by Voronoi index ⟨0, 3, 6, 4⟩.

Fig. 4 displays two histograms showing the population of different classes, both in the whole sample and in the strained region. Here we focus on four characteristic strains: the initial situation, that is 0% of strain; 10% of strain, corresponding to inhomogeneous regime, and finally 20% and 25% of strain, which correspond to the stage where the SB is completely formed (this is precisely the zone where the material will eventually fail). We can observe that in the case of the whole sample (Fig. 4(a)) the distribution is bimodal for all strains. Interestingly, for the case of the atoms in the strained region (Fig. 4(b)), at the 10% of strain the distribution becomes unimodal, being bimodal for lower and higher strain percentage. Note that at 10% of strain, all the classes have a significantly different behavior at the strained regions with respect to the whole material. Thus, one can interpret that at 10% there is a kind of transition, setting the beginning of the SB formation.

Another revealing analysis is to look at the types of polyhedra within the same class. We will focus our attention in two main classes, the 12-face and 13-face class polyhedra. It seems that the

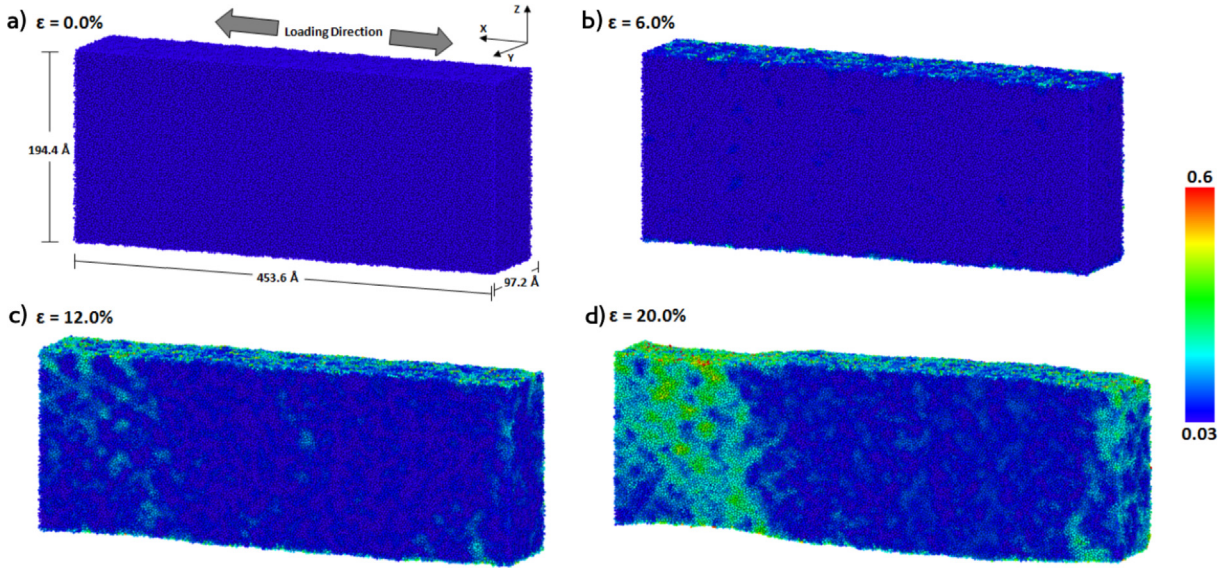

Fig. 2. Cross-section view at different strains of the $Cu_{50}Zr_{50}$ 1.008.000 atoms system at 300 K. Atoms are colored according to the shear strain.

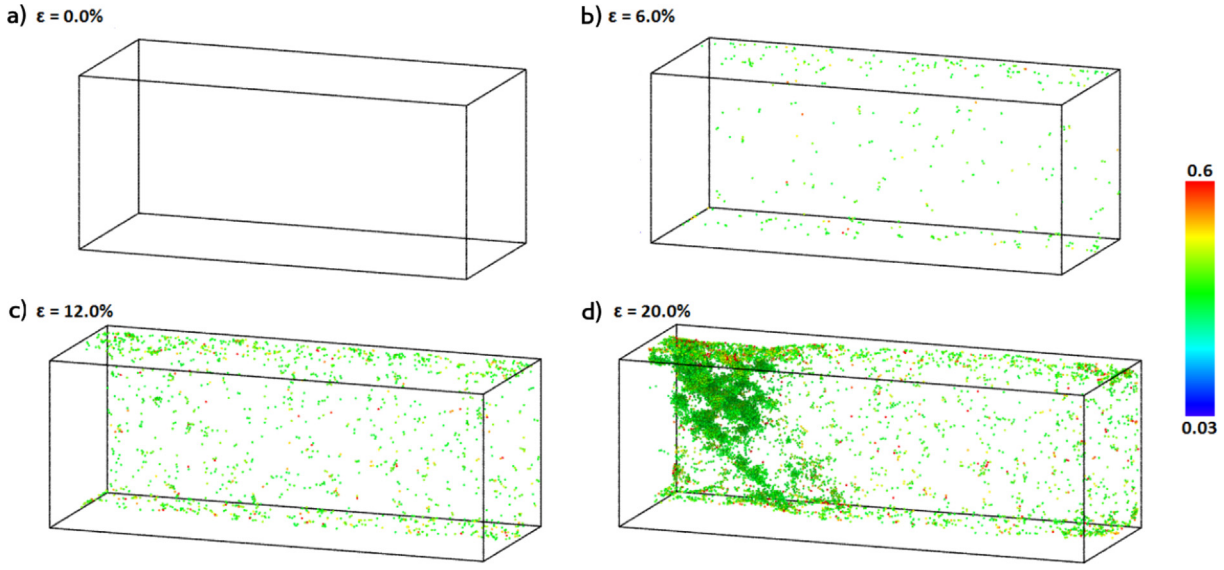

Fig. 3. Cross-section view of the shear band evolution in the $Cu_{50}Zr_{50}$ system at different strains. Only atoms with a shear strain greater than 0.3 are shown.

Table 1
Polyhedra evolution for different strains in the whole sample. The first column is the percentage of strain; the second column gives the number of different classes of polyhedra and the third column informs about the classes that predominate at that strain (most predominant left, less predominant right).

Strain %	Classes of polyhedra	Predominant class polyhedra
0%	34	12 13 15 16 14 11
5%	33	12 13 15 16 14 11
6%	35	13 12 15 16 14 17
10%	32	13 12 15 14 16 17
20%	29	13 12 15 14 16 17
25%	27	13 12 15 14 16 17

basic building blocks in CuZr glasses are those that belong to these classes [19]. Within these classes we will study the behavior of three characteristic polyhedra: the full icosahedra (FI), the distorted icosahedra (DI) and a kind of triskaidecahedra (T). The FI is represented by Voronoi index ⟨0, 0, 12, 0⟩ and has 12 pentagonal faces. Distorted icosahedra has index ⟨0, 2, 8, 2⟩, presenting 12 faces that not all of them are pentagons. Finally the triskaidecahedra has Voronoi index ⟨0, 3, 6, 4⟩ and represent a polyhedra with 13 faces: 6 tetragonal, 3 pentagonal and 4 hexagonal. These polyhedra has been used in previous works as an estimator of the topological changes that occurs in CuZr metallic glasses. For example, the full icosahedra units are characterized by an increased packing density [35] and high shear resistance [36]. Even more, the plastic deformation in the CuZr glass involves the destruction of this polyhedron [37].

Fig. 5 presents the changes of ⟨0, 0, 12, 0⟩, ⟨0, 2, 8, 2⟩ and ⟨0, 3, 6, 4⟩ according to the applied strain. Here we observe that in the 12-face class there are three regimes: below 3% of strain the number of this polyhedra does not change; then, between 3% and 10% of strain, the amount of this polyhedra decreases linearly; and after that, the amount remains constant. In the case of the T polyhedron, it decreases a little bit and then around 5% of strain, start to increase to reach (beyond 20% of strain) its initial value. Regarding to the ⟨0, 0, 12, 0⟩ polyhedron, the drastic decreases observed after 3% of strain

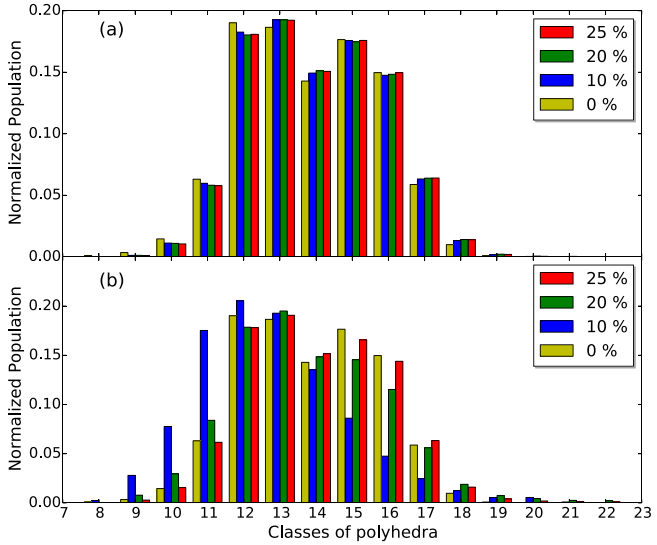

Fig. 4. Normalized population of polyhedra classes for different strains. (a) Distribution for the whole material; (b) distribution for the strained regions.

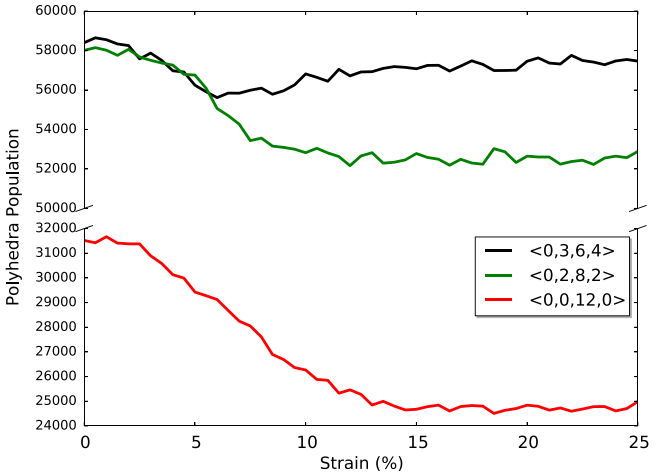

Fig. 5. Evolution of ⟨0, 0, 12, 0⟩, ⟨0, 2, 8, 2⟩ and ⟨0, 3, 6, 4⟩ polyhedra population according to applied strain. Population for the atoms in whole sample.

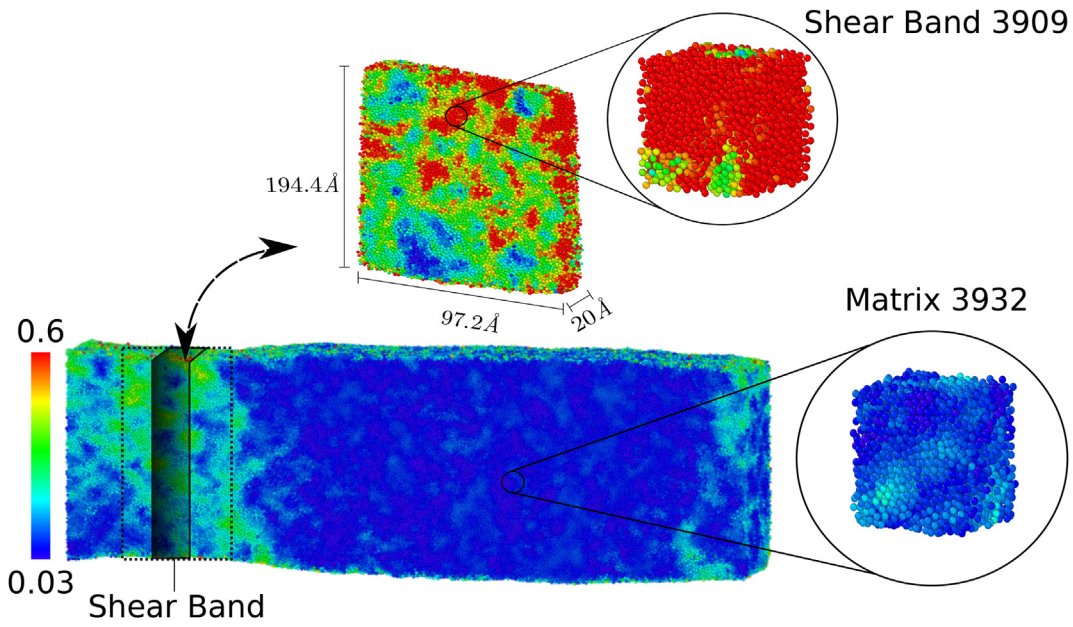

Fig. 6. Procedure to obtain the shear band sample and the matrix sample (see text for more detail). The system is colored according to the local atomic shear strain. (For interpretation of the references to color in this figure legend, the reader is referred to the web version of this article.)

is consistent with the onset of the plastic region observed in the stress–strain curve, Fig. 1, in good agreement with the fact that the FI is destroyed when plasticity begins [37].

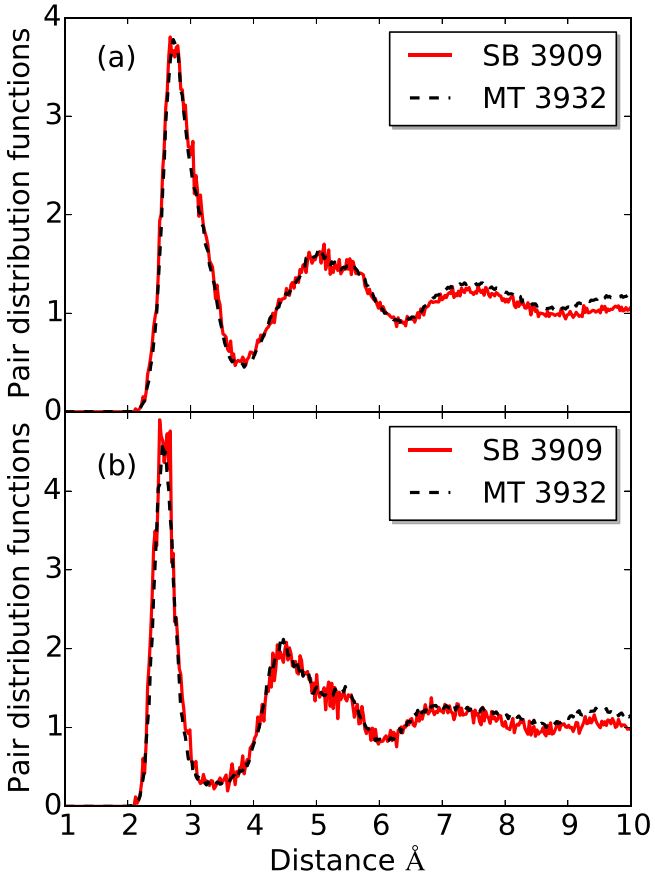

Fig. 7. Pair distribution function for the SB 3909 and MT 3932 samples. (a) Cu–Zr PDF and (b) Cu–Cu PDF.

It is interesting to compare our results of polyhedra evolution with previous works. For instance, in the work of Cheng et al. [35], they investigated the structure-plasticity correlation by monitoring the short-range order evolution during the deformation, and identifying the structure features that are predominant during the onset of plasticity. They found, for a $Cu_{64}Zr_{36}$ sample with periodic boundary conditions, that the full icosahedra $\langle 0, 0, 12, 0\rangle$ population decreases as the plastic flow initiate, while the other major type of polyhedra only change slightly or stay flat. This is the same trend that we found in our case, in spite of our test is in a nanowire. Thus, this kind of behavior seems to be robust.

In order to further investigate the atomic structure of the SB and the matrix (that is, the unstrained regions) we perform a detailed, comparative, analysis of both regions. In Fig. 6 it is shown how the samples were obtained. First, we identify the SB by visual inspection, and it corresponds to the regions inside the dashed line zone of Fig. 6. Then, from that zone, we extract a slice with high local atomic shear strain, represented by the shaded zone (see the arrow). From this slice of 20 Å thickness, we extract a cube 20 Å edge. This corresponds to a 3909-atoms system which we labeled "Shear Band 3909" (SB 3909). The same procedure is applied to the matrix system, resulting in a sample with the same volume, but with 3932

Table 2
Bond Angle Analysis (BAA) and Voronoi analysis for the SB 3909 and MT 3932 samples. FCC, HCP, BCC and ICO stand for Face Centered Cubic, Hexagonal Closed Package, Body Centered Cubic and Icosahedral structures, respectively.

Property	SB 3909	MT 3932
	%	%
BAA		
Other	71.6	72.1
FCC	1.2	1.4
HCP	14.0	13.9
BCC	11.4	10.6
ICO	1.8	2.0
Voronoi		
⟨0, 2, 8, 2⟩	4.2	4.2
⟨0, 3, 6, 4⟩	4.2	4.7
⟨0, 0, 12, 0⟩	1.8	2.0

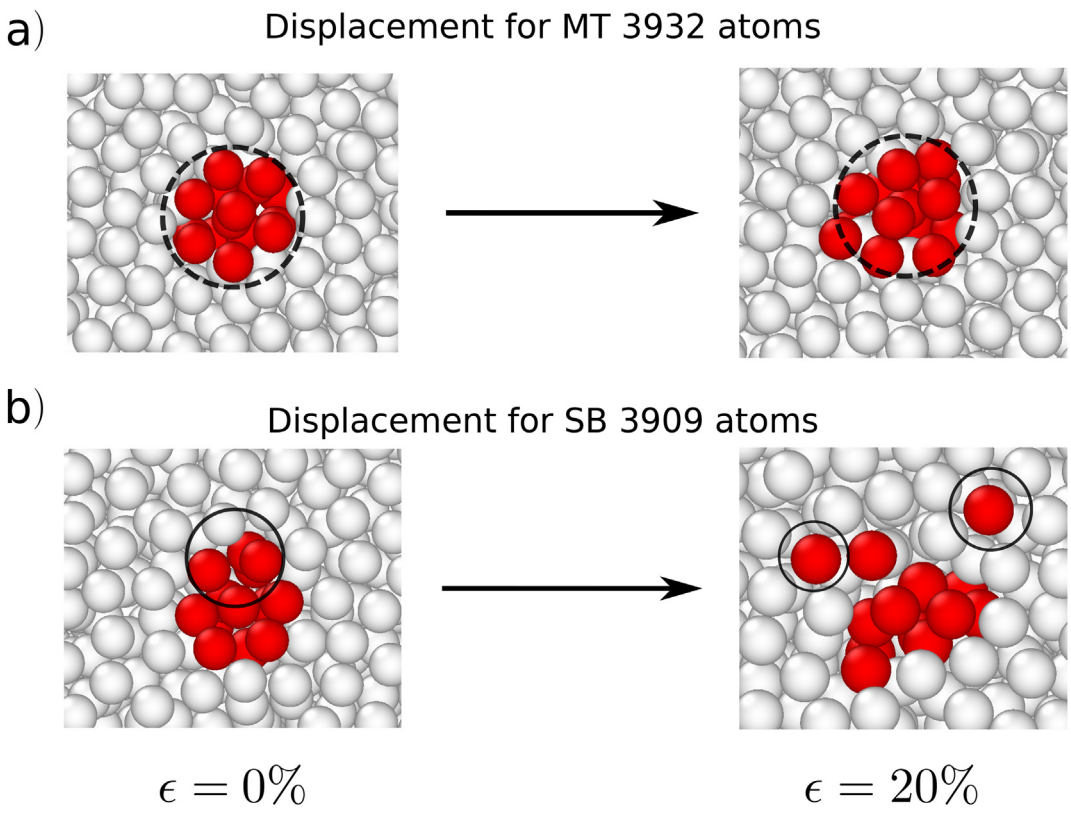

Fig. 8. Changes in cluster of CuZr atoms, colored in red, after 20% of strain. (a) the case of atoms at MT 3932, and (b) the case corresponding to SB 3909. (For interpretation of the references to color in this figure legend, the reader is referred to the web version of this article.)

atoms, labeled as "Matrix 3932" (MT 3932). These samples were analyzed by means of three structural diagnostics: Pair Distribution Function (PDF), Bond Angle Analysis (BAA) and Voronoi analysis.

Fig. 7 shows the PDF for the SB 3909 and for the MT 3932, Fig. 7(a) corresponding to the Cu–Zr PDF and Fig. 7(b) to the Cu–Cu PDF. It can be observed that both PDF are similar. The results of Bond Angle Analysis (BAA) and Voronoi analysis (Voronoi) are presented in Table 2. BAA give us information about the local environment of particles using the Ackland–Jones bond-angle method [38] and assigns a structure type (FCC, BCC, HCP etc.) to each atom.

Table 2 shows that the BAA for the SB 3909 and the MT 3932 gives almost the same results, where the main difference is presented for the BCC environment: while SB 3909 has 11.4% BBC atoms, MT 3932 has 10.6%. In the case of the Voronoi analysis, for the three characteristic polyhedra investigated, all of them present similar percentages in both samples. Note that although the region analyzed for SB 3909 corresponds to a zone with high local atomic shear strain, the short range order (SRO) for the atoms that belong to the sample is similar to the MT 3932 sample. Thus, both structures are practically indistinguishable according to the local structure analysis performed.

To see in detail what is really the difference between both regions, we focus our attention in a cluster of atoms. Fig. 8 presents the changes suffered for a cluster of atoms after 20% of strain. In Fig. 8(a) is displayed the case of atoms at MT 3932, and in Fig. 8(b), the case corresponding to SB 3909. We can see that after 20% of strain, in the first case the atoms of the cluster (red atoms) keep the same neighbors, but in the second case, there is two atom which are far away from the cluster and now those atoms have new neighbors. Interestingly, this is not indicative of any big changes in the local structure, as we reported in the previous structural analysis. That means that the changes occurred in the SB are more subtle and they are not captured by local structural diagnostics like PDF, BAA and Voronoi analysis.

4. Conclusions

We have presented a tensile test on CuZr metallic glass nanowire by means of molecular dynamics simulation. The stress–strain curve presents an elastic regime below 4% of strain, then an homogeneous deformation and after that an inhomogeneous deformation above 6% of strain. From the visualization of the simulation we can conclude that in the homogeneous deformation region the MG nanowire is composed by STZs, which coalesce around 10% of strain, forming the SB. According to our polyhedral distribution analysis, 10% of strain is a critical value, that set the beginning of the SB formation. A detailed atomic level study on the strained and unstrained regions, revealed that although the displacement of each atom with respect to its environment is very different, the short range order of both regions is similar.

Acknowledgments

M.S-M. thanks to CONICyT PhD fellowship No. 21140904. G.G. thanks to grant FONDECyT Chile 1120603 and Anillo ACT-1115.

References

[1] C. Suryanarayana, A. Inoue, Bulk Metallic Glasses, CRC Press, 2011.
[2] L. Tian, Y.-Q. Cheng, Z.-W. Shan, J. Li, C.-C. Wang, X.-D. Han, J. Sun, E. Ma, Approaching the ideal elastic limit of metallic glasses, Nat. Commun. 3 (2012) 609, http://dx.doi.org/10.1038/ncomms1619. http://www.nature.com/ncomms/journal/v3/n1/suppinfo/ncomms1619_S1.html.
[3] P. Zhao, J. Li, Y. Wang, Extended defects, ideal strength and actual strengths of

finite-sized metallic glasses, Acta Mater. 73 (0) (2014) 149–166, http://dx.doi.org/10.1016/j.actamat.2014.03.068. http://www.sciencedirect.com/science/article/pii/S1359645414002365.
[4] Crystallizing glassy issues, Nat. Mater. 14 (June 2015) 541, http://dx.doi.org/10.1038/nmat4319. http://www.nature.com/doifinder/10.1038/nmat4319.
[5] C.L. Kelchner, S.J. Plimpton, J.C. Hamilton, Dislocation nucleation and defect structure during surface indentation, Phys. Rev. B 58 (1998) 11085–11088, http://dx.doi.org/10.1103/PhysRevB.58.11085. http://link.aps.org/doi/10.1103/PhysRevB.58.11085.
[6] S.H. Oh, M. Legros, D. Kiener, G. Dehm, In situ observation of dislocation nucleation and escape in a submicrometre aluminium single crystal, Nat. Mater. 8 (2009) 95–100, http://dx.doi.org/10.1038/nmat2370. http://www.nature.com/nmat/journal/v8/n2/suppinfo/nmat2370_S1.html.
[7] A. Stukowski, K. Albe, Extracting dislocations and non-dislocation crystal defects from atomistic simulation data, Model. Simul. Mater. Sci. Eng. 18 (8) (2010) 085001. http://stacks.iop.org/0965-0393/18/i=8/a=085001.
[8] E. Ma, Tuning order in disorder, Nat. Mater. 14 (6) (2015) 547–552, http://dx.doi.org/10.1038/nmat4300. http://www.nature.com/doifinder/10.1038/nmat4300.
[9] C. Pampillo, Localized shear deformation in a glassy metal, Scr. Metall. 6 (10) (1972) 915–917, http://dx.doi.org/10.1016/0036-9748(72)90144-5. http://www.sciencedirect.com/science/article/pii/0036974872901445.
[10] W. Jiang, F. Pinkerton, M. Atzmon, Mechanical behavior of shear bands and the effect of their relaxation in a rolled amorphous al-based alloy, Acta Mater. 53 (12) (2005) 3469–3477, http://dx.doi.org/10.1016/j.actamat.2005.04.003. http://www.sciencedirect.com/science/article/pii/S1359645405002144.
[11] W.J. Wright, T.C. Hufnagel, W.D. Nix, Free volume coalescence and void formation in shear bands in metallic glass, J. Appl. Phys. 93 (3) (2003) 1432–1437, http://dx.doi.org/10.1063/1.1531212. http://scitation.aip.org/content/aip/journal/jap/93/3/10.1063/1.1531212.
[12] Q.-K. Li, M. Li, Atomic scale characterization of shear bands in an amorphous metal, Appl. Phys. Lett. 88 (24) (2006), http://dx.doi.org/10.1063/1.2212059. http://scitation.aip.org/content/aip/journal/apl/88/24/10.1063/1.2212059.
[13] C. Pampillo, H. Chen, Comprehensive plastic deformation of a bulk metallic glass, Mater. Sci. Eng. 13 (2) (1974) 181–188, http://dx.doi.org/10.1016/0025-5416(74)90185-2. http://www.sciencedirect.com/science/article/pii/0025541674901852.
[14] C.A. Schuh, T.C. Hufnagel, U. Ramamurty, Mechanical behavior of amorphous alloys, Acta Mater. 55 (12) (2007) 4067–4109, http://dx.doi.org/10.1016/j.actamat.2007.01.052. http://www.sciencedirect.com/science/article/pii/S135964540700122X.
[15] J. Wachter, G. Gutiérrez, A. Zúñiga, R. Palma, Buckling of CuZr-based metallic glasses nanowires: molecular dynamics study of surface effects, J. Mater. Sci. 49 (23) (2014) 8051–8056, http://dx.doi.org/10.1007/s10853-014-8512-9. http://dx.doi.org/10.1007/s10853-014-8512-9.
[16] Z.W. Shan, J. Li, Y.Q. Cheng, A.M. Minor, S.A. Syed Asif, O.L. Warren, E. Ma, Plastic flow and failure resistance of metallic glass: Insight from in situ compression of nanopillars, Phys. Rev. B 77 (2008) 155419, http://dx.doi.org/10.1103/PhysRevB.77.155419. http://link.aps.org/doi/10.1103/PhysRevB.77.155419.
[17] F. Shimizu, S. Ogata, J. Li, Theory of shear banding in metallic glasses and molecular dynamics calculations, Mater. Trans. 48 (11) (2007) 2923–2927.
[18] Y. Ritter, D. Opu, H. Gleiter, K. Albe, Structure, stability and mechanical properties of internal interfaces in $Cu_{64}Zr_{36}$ nanoglasses studied by {MD} simulations, Acta Mater. 59 (17) (2011) 6588–6593, http://dx.doi.org/10.1016/j.actamat.2011.07.013. http://www.sciencedirect.com/science/article/pii/S1359645411004782.
[19] Y. Ritter, K. Albe, Chemical and topological order in shear bands of $Cu_{64}Zr_{36}$ and $Cu_{36}Zr_{64}$ glasses, J. Appl. Phys. 111 (10) (2012), http://dx.doi.org/10.1063/1.4717748. http://scitation.aip.org/content/aip/journal/jap/111/10/10.1063/1.4717748.
[20] K. Albe, Y. Ritter, D. Opu, Enhancing the plasticity of metallic glasses: shear band formation, nanocomposites and nanoglasses investigated by molecular dynamics simulations, Mech. Mater. 67 (0) (2013) 94–103, http://dx.doi.org/10.1016/j.mechmat.2013.06.004 nanostructured Materials, http://www.sciencedirect.com/science/article/pii/S0167663613001117.
[21] M.I. Mendelev, D.J. Sordelet, M.J. Kramer, Using atomistic computer simulations to analyze X-ray diffraction data from metallic glasses, J. Appl. Phys. 102 (4) (2007), http://dx.doi.org/10.1063/1.2769157. http://scitation.aip.org/content/aip/journal/jap/102/4/10.1063/1.2769157.
[22] M.I. Mendelev, M.J. Kramer, R.T. Ott, D.J. Sordelet, D. Yagodin, P. Popel, Development of suitable interatomic potentials for simulation of liquid and amorphous Cu–Zr alloys, Philos. Mag. 89 (11) (2009) 967–987, http://dx.doi.org/10.1080/14786430902832773, 435YYTimes Cited:0Cited References Count:33, Pii 910503793. URL <GotoISI>://000265380600003.
[23] M. Li, C.Z. Wang, S.G. Hao, M.J. Kramer, K.M. Ho, Structural heterogeneity and medium-range order in Zr_xCu_{100-x} metallic glasses, Phys. Rev. B 80 (2009) 184201, http://dx.doi.org/10.1103/PhysRevB.80.184201. http://link.aps.org/doi/10.1103/PhysRevB.80.184201.
[24] H.L. Peng, M.Z. Li, W.H. Wang, C.-Z. Wang, K.M. Ho, Effect of local structures and atomic packing on glass forming ability in Cu_xZr_{100x} metallic glasses, Appl. Phys. Lett. 96 (2) (2010), http://dx.doi.org/10.1063/1.3282800. http://scitation.aip.org/content/aip/journal/apl/96/2/10.1063/1.3282800.
[25] G.J. Ackland, V. Vitek, Many-body potentials and atomic-scale relaxations in noble-metal alloys, Phys. Rev. B 41 (1990) 10324–10333, http://dx.doi.org/10.1103/PhysRevB.41.10324. http://link.aps.org/doi/10.1103/PhysRevB.41.10324.
[26] M.W. Finnis, J.E. Sinclair, A simple empirical n-body potential for transition metals, Philos. Mag. A 50 (1) (1984) 45–55, http://dx.doi.org/10.1080/01418618408244210.
[27] C. Wang, C. Wong, Structural properties of $Zr_xCu_{90x}Al_{10}$ metallic glasses investigated by molecular dynamics simulations, J. Alloys Compd. 510 (1) (2012) 107–113, http://dx.doi.org/10.1016/j.jallcom.2011.07.110. http://www.sciencedirect.com/science/article/pii/S0925838811017816.
[28] S. Melchionna, G. Ciccotti, B. Lee Holian, Hoover npt dynamics for systems varying in shape and size, Mol. Phys. 78 (3) (1993) 533–544, http://dx.doi.org/10.1080/00268979300100371.
[29] H.J.C. Berendsen, J.P.M. Postma, W.F. van Gunsteren, A. DiNola, J.R. Haak, Molecular dynamics with coupling to an external bath, J. Chem. Phys. 81 (8) (1984) 3684–3690, http://dx.doi.org/10.1063/1.448118. http://link.aip.org/link/?JCP/81/3684/1.
[30] S. Plimpton, Fast parallel algorithms for short-range molecular dynamics, J. Comput. Phys. 117 (1) (1995) 1–19, http://dx.doi.org/10.1006/jcph.1995.1039. http://www.sciencedirect.com/science/article/pii/S002199918571039X.
[31] A. Stukowski, Visualization and analysis of atomistic simulation data with ovitothe open visualization tool, Model. Simul. Mater. Sci. Eng. 18 (1) (2010) 015012. http://stacks.iop.org/0965-0393/18/i=1/a=015012.
[32] S. Davis, C. Loyola, F. Gonzlez, J. Peralta, Las palmeras molecular dynamics: a flexible and modular molecular dynamics code, Comput. Phys. Commun. 181 (12) (2010) 2126–2139, http://dx.doi.org/10.1016/j.cpc.2010.08.030. http://www.sciencedirect.com/science/article/pii/S001046551000336X.
[33] C.H. Rycroft, Voro++: a three-dimensional voronoi cell library in c++, Chaos: an interdisciplinary, J. Nonlinear Sci. 19 (4) (2009), http://dx.doi.org/10.1063/1.3215722. http://scitation.aip.org/content/aip/journal/chaos/19/4/10.1063/1.3215722.
[34] Y. Cheng, E. Ma, Atomic-level structure and structureproperty relationship in metallic glasses, Prog. Mater. Sci. 56 (4) (2011) 379–473, http://dx.doi.org/10.1016/j.pmatsci.2010.12.002. http://www.sciencedirect.com/science/article/pii/S0079642510000691.
[35] Y. Cheng, A. Cao, H. Sheng, E. Ma, Local order influences initiation of plastic flow in metallic glass: effects of alloy composition and sample cooling history, Acta Mater. 56 (18) (2008), http://dx.doi.org/10.1016/j.actamat.2008.07.011. http://www.sciencedirect.com/science/article/pii/S1359645408004850.
[36] J.-C. Lee, K.-W. Park, K.-H. Kim, E. Fleury, B.-J. Lee, M. Wakeda, Y. Shibutani, Origin of the plasticity in bulk amorphous alloys, J. Mater. Res. 22 (2007) 3087–3097, http://dx.doi.org/10.1557/JMR.2007.0382. http://journals.cambridge.org/article_S0884291400026595.
[37] S.-C. Lee, M.-Y. Huh, H.-J. Kim, J.-C. Lee, Extraordinary plasticity of an amorphous alloy based on atomistic-scale phase separation, Mater. Sci. Eng. A 485 (12) (2008), http://dx.doi.org/10.1016/j.msea.2007.08.068. http://www.sciencedirect.com/science/article/pii/S0921509307016127.
[38] G.J. Ackland, A.P. Jones, Applications of local crystal structure measures in experiment and simulation, Phys. Rev. B 73 (2006) 054104, http://dx.doi.org/10.1103/PhysRevB.73.054104. http://link.aps.org/doi/10.1103/PhysRevB.73.054104.